

1 **Genomic instability and *TP53* genomic alterations associate with poor anti-**  
2 **proliferative response and intrinsic resistance to aromatase inhibitor treatment**

3  
4 Eugene F. Schuster<sup>1,2</sup>, Pascal Gellert<sup>1,2</sup>, Corrinne V. Segal<sup>1,2</sup>, Elena López-Knowles<sup>1,2</sup>,  
5 Richard Buus<sup>1,2</sup>, Maggie Chon U Cheang<sup>3</sup>, James Morden<sup>3</sup>, John Robertson<sup>4</sup>, Judith M.  
6 Bliss<sup>3</sup>, Ian Smith<sup>2</sup>, Mitch Dowsett<sup>1,2</sup> & POETIC Trial Management Group and Trialists

7  
8 1 - Breast Cancer Now Research Centre at The Institute of Cancer Research, 237 Fulham  
9 Road, London SW3 6JB, UK

10 2 - Ralph Lauren Centre for Breast Cancer Research, Royal Marsden Hospital, Fulham  
11 Road, London SW3 6JJ, UK

12 3 - Clinical Trials and Statistics Unit at The Institute of Cancer Research, 15 Cotswold  
13 Road, London SM2 5NG, UK

14 4 - University of Nottingham, Derby Road, Nottingham NG7 2UH, UK

15

16

17 **Funding:** This work was supported by the Mary-Jean Mitchell Green Foundation, Breast  
18 Cancer Now and the NIHR RM/ICR Biomedical Research Centre. The POETIC trial  
19 (C1491/A8671/CRUK/07/015, C1491/A15955 and C406/A8962), from which samples were  
20 obtained for this study, was supported by Cancer Research UK (CRUK/07/015) as is ICR-  
21 CTSU through its core programme grant. POETIC was registered with ISRCTN registry  
22 (ISRCTN63882543).

23

24 **Corresponding Author:**

25 Eugene F. Schuster, Ph.D.  
26 The Institute of Cancer Research  
27 237 Fulham Road  
28 London SW3 6JB, UK  
29 Tel: +44 (0)20 7808 2619  
30 Email: gschuster@icr.ac.uk

31

32 **Running Head:**

33 **Genomic instability and resistance to aromatase inhibitor treatment**

34

35 **Conflicts of Interests:** JR is employed by Oncimmune. JR holds stock in Oncimmune and  
36 FaHRAS. JR received honoraria from AstraZeneca, Bayer and Amgen. JR receives  
37 research funding from Oncimmune. JR holds patents from Oncimmune and is in the  
38 speakers' bureau of AstraZeneca. MD is a paid adviser to Radius and receives financial  
39 benefits from the Institute of Cancer Research's Rewards for Inventors Scheme; MD  
40 receives funding from Pfizer and Radius. The remaining authors declare no competing  
41 financial interests.

42 **Key objective:** Our study was focused on understanding the link between somatic copy  
43 number alterations (SCNAs) and intrinsic resistance to aromatase inhibition (AI) therapy  
44 and we observed tumors with high levels SCNAs had intrinsic resistance to therapy.

45

46 **Knowledge generated:** There is a well established link between high genomic instability  
47 (GI) and *TP53* mutations and resistance to cancer treatment; however, we are the first to  
48 show that primary ER+ tumors with high GI have an intrinsic resistance to treatment that  
49 can be measured after a short two-week AI treatment. High GI tumors do not require time  
50 to evolve resistance to estrogen deprivation therapy as they already have de novo  
51 resistance to treatment.

52

53 **Revelance:** Estrogen deprivation therapy with AI treatment is highly effective in ER+  
54 breast cancer (BC), but more than 20% of postmenopausal women with early-stage BC  
55 suffer a relapse. The POETIC phase III trial with 2-weeks of perioperative AI therapy  
56 offers the opportunity to identify mechanisms and biomarkers of intrinsic AI resistance, and  
57 in the POETIC study up to 20% of tumors showed resistance to AI treatment after just 2  
58 weeks of treatment. The results show high genomic instability (GI) is associated with AI  
59 resistance and detection of copy number alterations and mutations in *TP53* are predictive  
60 of high GI. Validation of these results in a larger study would provide a framework for  
61 better stratifying patients into high risk of AI-resistance that are likely to benefit from added  
62 or alternative treatment.

63

64

65 **Abstract**

66

67 **Purpose:** While aromatase inhibition (AI) is an effective treatment for estrogen receptor-  
68 positive postmenopausal breast cancer (BC) resistance is common and incompletely  
69 explained. Genomic instability (GI) as measured by somatic copy number alterations  
70 (SCNAs) is important in BC development and prognosis. SCNAs to specific genes may  
71 drive intrinsic resistance, or high GI may drive tumor heterogeneity allowing differential  
72 response across the tumors and surviving cells to rapidly evolve resistance to treatment.  
73 We therefore evaluated the relationship between SCNAs and intrinsic resistance to  
74 treatment as measured by a poor anti-proliferative response.

75 **Patients and Methods:** SCNAs were determined by SNParray in baseline and surgery  
76 core-cuts from 73 postmenopausal patients randomized to receive 2 weeks' pre-operative  
77 AI or no AI in the POETIC trial. Fifty-six samples from the AI-group included 28 poor  
78 responders (PrRs, <60% reduction in Ki67) and 28 good responders (GdRs, >75%  
79 reduction in Ki67). Exome sequencing was available for 72 pairs of samples.

80 **Results:** GI correlated with Ki67 expression at both baseline ( $P=0.0003$ ) and at surgery  
81 ( $P= 0.0002$ ), and GI was higher in PrRs ( $P=0.048$ ). The SCNA with the largest difference  
82 between GdRs and PrRs was loss of heterozygosity (LOH) observed at 17p (FDR=0.08),  
83 which includes *TP53*. Nine of 28 PrRs had loss of wildtype *TP53* due to mutations and  
84 LOH compared to 3 of 28 GdRs. In PrRs, somatic alterations of *TP53* were associated  
85 with higher GI, higher baseline Ki67 and greater resistance to AI treatment compared to  
86 wildtype *TP53*.

87 **Conclusion:** We observed that primary tumors with high GI have an intrinsic resistance to  
88 AI treatment and do not require further evolution to develop resistance to estrogen  
89 deprivation therapy.

90 **Introduction**

91 Estrogen deprivation is the major treatment strategy for hormone-dependent breast cancer  
92 (BC) and typically involves agents that inhibit aromatase, the enzyme catalyzing the  
93 conversion of androgens to estrogens. Despite near complete suppression of circulating  
94 estrogen levels by aromatase inhibitor (AI) treatment, acquired and *de novo* resistance to  
95 AI is common<sup>1</sup>. There are few pre-treatment biomarkers for AI resistance and mechanisms  
96 of resistance are incompletely understood<sup>2</sup>.

97

98 Mutations and somatic copy number alterations (SCNAs) can play important roles in  
99 activating oncogenes or inactivating tumor suppressors, and BC is characterised by  
100 multiple recurrent SCNAs and few recurrent mutations<sup>3</sup>. We have previously shown that  
101 *TP53* mutations occur at a higher rate in tumors with poor response to AI treatment  
102 suggesting these patients received less benefit from AI<sup>4</sup> but SCNAs to specific genes may  
103 also play an important role in AI resistance<sup>5</sup>. It is known that non-specific genomic  
104 alterations like high genomic instability (GI) is associated with poor prognosis and probably  
105 due at least partly to tumor heterogeneity allowing some cells to survive and evolve  
106 resistance to treatment<sup>6</sup>. There is evidence in other solid tumors for an association of high  
107 GI and intrinsic resistance to chemotherapy<sup>7</sup>. However, there are few studies of GI and  
108 response to endocrine treatment. The aim of this work was therefore to determine if  
109 genome-wide measures of SCNAs (*i.e.* genomic instability - GI) and/or focal SCNAs are  
110 associated with intrinsic resistance to AI treatment.

111

112 Response to AI treatment can be measured by change in the proliferation marker Ki67,  
113 following 2-4 weeks of presurgical therapy, and AI resistance in primary tumors can be  
114 characterized and defined by limited or no Ki67 response to AI treatment<sup>8-10</sup>. This change

115 in Ki67 has been found to predict benefit from endocrine therapy better than clinical  
116 response<sup>10</sup>. We therefore extended our earlier study on the relationship between  
117 mutations and resistance to AIs in the pre-surgical Perioperative Endocrine Therapy—  
118 Individualising Care (POETIC) trial. We used SNParray technology to identify SCNAs and  
119 included paired baseline and surgery samples to assess the degree of intra-tumoral  
120 heterogeneity and selection during AI treatment.

121

## 122 **Methods**

### 123 *Patients and tissues*

124 The POETIC trial (CRUK/07/015) is a pre-surgical randomized study with 4,486 post-  
125 menopausal patients receiving non-steroidal AI (anastrozole 1 mg/day or letrozole  
126 2.5 mg/day) or no treatment (2:1) two-weeks before surgery<sup>11</sup>. Core-cut biopsies (14-G)  
127 were collected from c.15% of patients into RNA<sup>later</sup> (Qiagen). Whole blood was collected  
128 for germline DNA analysis. The trial was approved by the NRES Committee London-South  
129 East. Patients gave informed consent for DNA analysis.

130

### 131 *Biomarker analyses*

132 Ki67% staining was centrally analyzed on formalin-fixed samples as previously described<sup>8</sup>.  
133 HER2 status was measured locally. Ki67 and HER2 results are shown in Supplementary  
134 Table 1.

135

### 136 *Sample Selection*

137 DNA was extracted from 192 baseline/surgery samples from the subset of POETIC ER+  
138 tumors stored in RNA<sup>later</sup> and matching blood controls from 73 patients with baseline Ki67  
139 scores greater than 5%. Poor responders (n=28) were defined as having a Ki67 decrease

140 of <60% between baseline and surgery, and good responders (n=28) with >75% Ki67  
141 decrease (Supplemental Figure 1). Patients with intermediate Ki67 decrease between 60-  
142 75% were not considered. Exome sequencing was available for 72 tumors from a previous  
143 study<sup>4</sup>. Samples from 17 patients who received no-AI were also analysed to ensure that  
144 changes in SCNAs ascribed to AI treatment were not artefactual. Aliquots were taken from  
145 10 tumor DNA samples and assessed as technical replicates (Supplemental Figure 1).

146

#### 147 *DNA extractions*

148 8- $\mu$ m sections were taken from RNAlater-stored core-cuts embedded in OCT (Cryo-M-  
149 Bed, Bright Instruments, UK) and stained with Nuclear Fast Red (0.1% (w/v)). Needle  
150 microdissection was used to achieve >60% pure tumor cells when necessary. DNA was  
151 extracted from the sections using the DNeasy Tissue and Blood kit (Qiagen), and from  
152 peripheral blood using the EZ1 system (LifeTechnologies).

153

#### 154 *SNParray Analysis*

155 Illumina Human OmniExpress Exome BeadChip v.3 was used to generate genotype and  
156 intensity data for blood and tumor samples, and ASCAT<sup>12</sup> for the estimate of ploidy,  
157 fraction of tumor cells and copy number alterations (CNA) in the tumor samples. Two  
158 samples did not pass ONCOSNP QC<sup>13</sup> and visual inspection of the SNP-array data. Ploidy  
159 and purity using default parameters and a range of higher segmentation penalties were  
160 estimated with ASCAT and OncoSNP. The segmentation penalty in ASCAT was increased  
161 (22-samples) or the estimate of ploidy and purity from OncoSNP was used in ASCAT (4-  
162 samples) to generate SCNA calls that best described the data. For five samples, germline  
163 genotype predictions generated by ASCAT were due to contamination or QC failure of  
164 blood controls. Bedtool multiintersect<sup>14</sup> was used to identify 47807 non-overlapping

165 segments from all samples. Data has been deposited in the European Genome-phenome  
166 Archive (EGAS00001001940).

167

### 168 *Measures of Genomic Instability*

169 Chromosomal gains and losses were determined relative to estimates of tumor ploidy by  
170 ASCAT (sum of major and minor allele calls minus tumor ploidy rounded to nearest  
171 integer). Loss of heterozygosity (LOH) was assigned when the estimated copy number  
172 was zero for the minor allele (LOH). Genomic Instability (GI) was defined as the  
173 percentage of the genome with SCNAs calculated by summing the total basepairs (bp) of  
174 segments with gains, loss or LOH relative to paired normal blood control samples for each  
175 tumor sample and dividing by the size of the genome ( $3 \times 10^9$ bp).

176

### 177 *Intrinsic Subtypes*

178 PAM50 intrinsic subtypes were determined for 36 tumors<sup>15</sup>. Details are available in  
179 Supplemental Table 1.

180

### 181 *Statistical methods*

182 Mann-Whitney,  $F$ , chi-squared, Pearson's correlation (Pearson's), Fisher's exact tests  
183 (Fisher's), and multiple correction by Benjamini-Hochberg method<sup>16</sup> (FDR) were also  
184 carried out using R with the wilcox.test, var.test, chisq.test, cor.test, fisher.test, p.adjust  
185 functions, respectively. Fisher's exact tests were one-sided and remaining reported p-  
186 values were two-sided tests unless otherwise specified. Boxplot plots were generated with  
187 the boxplot function in R to show median, interquartile and range of values excluding  
188 outliers.

189

## 190 **Results**

### 191 **SCNA characteristics in the overall population**

192 SCNAs were identified in 28 patients with tumors classified as PrRs, 28 classified as GdRs  
193 and 17 tumors from the no-treatment control group (Figure 1A). The median percent of the  
194 genome with SCNAs was 46% for all tumors with a single representative tumor sample  
195 chosen from matched baseline, surgery or technical replicate samples to calculate the  
196 median percentage of SCNAs. The median percent of the genome with gains relative to  
197 tumor ploidy, losses relative to tumor ploidy, and LOH was 15%, 16%, and 15%,  
198 respectively (Figure 1B, Supplemental Table 2). Highly recurrent SCNAs (gains at 1q, 16p,  
199 20q and 8q, and losses/LOH at 11q 16q, 17p and 8p) occurred in >50% of all  
200 representative samples (Supplemental Figure 2A-D). The majority of sites with losses  
201 overlapped with LOH (Supplemental Figure 2E), as expected<sup>17,18</sup>.

202

### 203 **Intratumoral heterogeneity of SCNAs**

#### 204 *Overlap of SCNAs between paired core-cuts*

205 Discordance between baseline and surgery time points was significantly greater than  
206 differences between technical replicate samples taken from the same DNA extraction  
207 (Supplemental Figure 2F). Discordance in SCNAs was observed in >10% of the genome  
208 in only one pair of technical replicate samples; notably, these samples had the highest GI  
209 with >90% of the genome with SCNAs (P088 samples, Supplemental Figure 3A).

210

211 Overall SCNA calls in baseline and surgery AI pairs were very similar (Supplemental  
212 Figure 3) with the median overlap for SCNAs at 87% and 88% for 33 baseline/surgery AI  
213 pairs and 11 no-AI pairs respectively. There was no significant difference between the  
214 frequency of discordant SNCA calls between baseline and surgery AI pairs after correction

215 for multiple testing and only 4% of 47807 non-overlapping regions have >10% more  
216 events in baseline or surgery samples (>4 additional SCNA events in the baseline or  
217 surgery samples in the 33 pairs)(Supplemental Figure 4). Much larger sample sizes are  
218 required to determine if these regions are significantly different between baseline and  
219 surgery.

220

### 221 *Concordance of SCNAs between paired core-cuts*

222 For pairs of baseline and surgery samples, the median percentage of the genome with  
223 discordant SCNA calls was 5% (Figure 1C), and discordance between samples was  
224 associated with the percentage of the genome with SCNAs (Supplemental Figure 5).  
225 There was only one paired set of core-cuts in which discordant SCNAs were greater than  
226 the SCNAs shared between the pair of samples, suggesting two independently evolved  
227 tumors (Supplemental Figure 6).

228

### 229 *Discordance in PrR and GdR paired samples*

230 There was a trend for PrRs to have more discordant SCNAs between paired samples than  
231 GdRs (average 10% in PrRs and 6% in GdRs) but this difference was not significant.  
232 However, the variance in the percent of the genome with discordant SCNAs was  
233 significantly greater in PrRs than GdRs ( $P < 10^{-6}$ ,  $F$  test) (Figure 1D). These data indicate  
234 that the tumors with the highest topographic heterogeneity in SCNAs were more frequent  
235 among the PrRs.

236

### 237 **Intrinsic subtypes**

238 PAM50 intrinsic subtype calls<sup>15</sup> were performed on 36 baseline tumors. There is an  
239 enrichment of poor prognosis intrinsic subtypes (PrR non-luminal/luminal-B ) in PrR

240 samples (64%) compared to GrR (20%); however, >30% of measured PrR samples are  
241 luminal-A subtypes suggesting intrinsic subtyping is not fully capturing the higher risk of  
242 recurrence in these samples (Supplemental Table 1).

243

## 244 **Inter-tumoral heterogeneity in SCNAs**

### 245 *Comparison between PrRs and GdRs in percent of genome altered*

246 Given the overall concordance between baseline and surgery core-cuts in SCNAs and the  
247 results of previous observations of minimal impact of AI treatment on mutation counts<sup>4</sup>, we  
248 merged all the SCNA events from multiple samples from the same tumor to represent the  
249 SCNAs events in that tumor (merged 35-baseline and surgery; 9-baseline, surgery and  
250 technical replicates; 1-baseline technical replicates). The GI was higher in the 28 PrR  
251 combined samples than the 28 GdR combined samples ( $P=0.048$ , Mann-Whitney) and GI  
252 was significantly correlated with baseline ( $r=0.41, P=0.0003$ , Pearson's) and surgery  
253 ( $r=0.48, P=0.0002$ , Pearson's) Ki67 (Figure 2).

254

### 255 *Comparison of SCNAs between PrRs or GdRs*

256 The percentage of a chromosomal arm with gains, losses and LOH was calculated, and  
257 PrRs showed a significantly higher percentage of gains in chromosome 6p, losses in 5q,  
258 and LOH in 10q, 17p, and 19p (FDR < 0.1, one-sided Mann-Whitney) (Figure 3A-C,  
259 Supplemental Figure 7). The largest difference in percentage values (mean and median  
260 values) for arms between GdRs and PrRs was observed in LOH at 17p (Figure 3D-G),  
261 followed by LOH in 8p and gains in 8q. There were no chromosomal arms with significantly  
262 greater gains, losses or LOH in GdRs.

263

264 Analysis of smaller regions, based on the 47807 non-overlapping segments, revealed the  
265 most significant differences in gains were observed at 10p12.31 and 10p13 ( $P=0.0004$ ,  
266 Fisher's), losses at 5q11.2 ( $P=0.0002$ ), and LOH at 17p13.3 ( $P=0.0005$ ). These regions  
267 had approximately 40% more events in PrRs (13 to 10 more SCNA events in the 28 PrR  
268 samples than GrRs) but were not significant after multiple correction (Supplemental Figure  
269 8A).

270

### 271 ***TP53* alterations**

#### 272 *Occurrence of TP53 mutations and LOH in cohort*

273 Our previous work from exome sequencing showed PrRs and *TP53* mutations associated  
274 with a higher mutational load and that the mutational load was correlated with Ki67 levels  
275 at a surgery after 2-weeks of AI treatment<sup>4</sup>. We did not observe a significant correlation  
276 between the percent of the genome with SCNAs and mutational load, but we did observe  
277 greater GI in tumors with *TP53* mutations (Figure 4E).

278

279 As expected for a tumor suppressor, LOH at the *TP53* locus in 17p was associated with  
280 *TP53* mutations across all tumors (driving loss of the functioning copy of the tumor  
281 suppressor gene) ( $P=0.004$ , Fisher's). Of the 17 patients with *TP53* mutations in baseline  
282 or surgery samples, 15 had LOH at the *TP53* locus (9-PrRs, 5-GdRs, 3-Controls). All nine  
283 PrR samples and three out of five GrR samples with *TP53* mutations also had LOH at the  
284 *TP53* locus. There was a significant enrichment of *TP53* genomic alterations in PrRs  
285 ( $P=0.03$ , Fisher's) and significant difference in the distribution of *TP53* genetic alterations  
286 between PrRs and GdRs ( $P=0.02$ , Chi-squared) (Figure 4A).

287

#### 288 *AI resistance and TP53 status*

289 Within the PrR group, samples with no LOH and  $TP53^{WT}$  had the best anti-proliferative  
290 response to AI compared with samples with  $TP53^{WT}+LOH$  and  $TP53^{MUT}+LOH$  as  
291 measured by the change in Ki67 ( $P=0.01$  and  $P=0.05$  respectively, Mann-Whitney) (Figure  
292 4B). The difference in the change in Ki67 between  $TP53^{WT}+LOH$  and  $TP53^{MUT}+LOH$  was  
293 not significant but there were significant differences between  $TP53^{WT}+LOH$  and  
294  $TP53^{MUT}+LOH$  for baseline Ki67 scores ( $P=0.02$ ), for surgery Ki67 scores ( $P=0.04$ ) and for  
295 the percentage of the genome with SCNAs ( $P=0.0004$ ), (Figure 4B-E).

296

### 297 *Impact of HER2 status*

298 There were seven HER2 positive samples in the PrR group and none in the GdR group.  
299 HER2 positive samples had a significantly higher percentage of the genome with gains in  
300 copy number compared to HER2-negative PrR samples ( $P=0.03$ , Mann-Whitney) but did  
301 not have significantly higher percentage of SCNAs in general, losses or LOH  
302 (Supplemental Figure 8B-E). The results with HER2-negative cases were similar to those  
303 with all samples with the most significant differences between PrRs and GdRs being loss  
304 at 5q and LOH at 17p for HER2-negative samples (Supplemental Figures 8F-G, 9-10).  
305 There was also a significant enrichment of TP53 genomic alterations in PrRs ( $P=0.02$ ,  
306 Fisher's) and significant difference in the distribution of TP53 genetic alterations between  
307 PrRs and GdRs in HER2-negative samples ( $P=0.03$ , Chi-squared) (Supplemental Figure  
308 10C).

309

## 310 **Discussion**

311 Our primary goal was to identify global and focal SCNAs that were associated with the  
312 anti-proliferative response of ER+ BC to short-term estrogen deprivation using AIs. Our  
313 selection of samples from >3000 patients in the AI-group from the POETIC study aimed to

314 exploit this large study to understand good/poor response to AI treatment in a general ER+  
315 BC population but not to represent the trial population *per se*. The sampling of tumors  
316 before and after 2-weeks of AI treatment allowed the impact of tissue heterogeneity to be  
317 assessed, and prior exome sequencing gave the opportunity to integrate the SCNA and  
318 mutation data to better understand intrinsic resistance. While the number studied seems  
319 modest, the ability to assess response in individual tumors allows much greater confidence  
320 with molecular associations that larger studies with time to recurrence. HER2 positivity  
321 was enriched in the PrPs, as previously noted<sup>4</sup>, but the genomic changes were similar in  
322 HER2-negative cases and the overall population.

323

324 The lack of recurrent alterations specific to only baseline or surgery in AI-treated samples  
325 indicates a limited impact and selection for SCNAs after 2-weeks of AI treatment in line  
326 with other studies<sup>4,19</sup>. Notably, mean tumor volume did not change significantly in the  
327 nearly 3,000 POETIC AI-treated patients within the 2-week treatment window (data not  
328 shown) indicating little opportunity for selection of resistant cells in that time. Reduced  
329 heterogeneity might be observed from longer treatment<sup>20</sup>. These data therefore indicate  
330 that a small biopsy before or after short-term AI treatment is likely to be representative of  
331 the whole tumor for most BCs; however for tumors with high GI and greater heterogeneity,  
332 multiple biopsies may be necessary to capture all genomic alterations.

333

334 There is a large body of evidence to associate GI poor outcomes in solid tumors<sup>6</sup>, and  
335 incorporation of GI scores can greatly improve molecular prognostic models for BC<sup>21,22</sup>. It  
336 is not known if high GI and greater tumor heterogeneity allows the few surviving tumors to  
337 evolve resistance to AI treatment or if there is intrinsic resistance to AI in these tumors.  
338 Our data here support the latter with tumors with high GI showing *de novo* resistance to AI

339 therapy as measured by a poor Ki67 response after two weeks of treatment, a validated  
340 intermediate marker of benefit from endocrine therapy<sup>10</sup>. This also suggests that GI not  
341 only has prognostic value but also predicts which postmenopausal ER+ primary tumors  
342 are likely to be resistant to AI therapy.

343

344 LOH in 17p was significantly SCNA associated with poor Ki67 change, and LOH was  
345 significantly greater in PrR tumors compared to GdRs in HER2-negative tumors and the  
346 overall population. This region encodes for several cancer driver genes including *TP53*, a  
347 key regulator of cellular processes controlling proliferation and genomic stability. LOH and  
348 mutations in *TP53* has been shown to result in worse outcomes<sup>23</sup> and we have now shown  
349 that it is also associated with poor anti-proliferation response to AI and intrinsic resistance  
350 to treatment. Clearly there are other factors besides *TP53* that can modulate GI and AI  
351 resistance, and GI is significantly inversely correlated with the average expression of the  
352 ER-regulated genes *TFF1*, *GREB1*, *PGR* and *PDZJK1* in ER+ tumors from METABRIC<sup>24</sup>  
353 ( $r=-0.24, P<10^{-16}$ , Pearson's) suggesting other factors besides ER are driving proliferation  
354 and resistance to AI in tumors with high GI. Even in tumors with high ER expression and  
355 good prognosis, *TP53* genomic alterations can results in worse outcomes (Supplemental  
356 Figure 11).

357

358 Recent work by other groups has associated mutations in DNA repair pathways<sup>25</sup> or  
359 mismatch repair pathways<sup>19</sup> and co-amplification of *FGFR1* and *CCND1*<sup>5</sup> with resistance  
360 to AI treatment, but we have not observed enrichment of these genomic alterations in our  
361 PrRs. This may be due to small samples sizes in each study and additional differences in  
362 how AI resistance is classified: we classified response/resistance based on changes of  
363 Ki67 between baseline and AI-treated tumors since this dynamic assessment relates to

364 benefit from treatment. Others have used the level of residual Ki67 in AI-treated tumors as  
365 the endpoint to define resistance which reflects residual risk of recurrence on AI. Notably,  
366 a patient with a large reduction in proliferation after treatment has clearly benefited from  
367 and responded to AI treatment regardless of her residual risk based on Ki67  
368 measurements at surgery<sup>26</sup>.

369

370 We conclude that the poor prognosis of ER+ postmenopausal tumors associated with high  
371 GI, *TP53* LOH and *TP53* mutations is at least in part due to intrinsic resistance of these  
372 tumors to AI therapy. The short two-week AI treatment can reveal poor anti-proliferative  
373 response in these primary tumors indicating that they continue to proliferate in an estrogen  
374 deprived environment and do not require further evolution to enable the tumor to resist  
375 treatment. It is not clear if high GI or *TP53* genomic alterations directly play a role in AI  
376 resistance or if these are biomarkers for other drivers of resistance. Further analysis of the  
377 >3000 AI-treated patients from POETIC may reveal additional links between GI, *TP53* and  
378 AI resistance and lead to better treatment for those patients with high GI and intrinsic  
379 resistance to AI treatment.

380

## 381 **References**

- 382 1. Miller WR, Larionov A, Renshaw L, et al: Gene expression profiles differentiating  
383 between breast cancers clinically responsive or resistant to letrozole. *J Clin Oncol* 27:1382-7,  
384 2009
- 385 2. Lopez-Knowles E, Wilkerson PM, Ribas R, et al: Integrative analyses identify  
386 modulators of response to neoadjuvant aromatase inhibitors in patients with early breast  
387 cancer. *Breast Cancer Res* 17:35, 2015
- 388 3. Ciriello G, Miller ML, Aksoy BA, et al: Emerging landscape of oncogenic  
389 signatures across human cancers. *Nat Genet* 45:1127-33, 2013
- 390 4. Gellert P, Segal CV, Gao Q, et al: Impact of mutational profiles on response of  
391 primary oestrogen receptor-positive breast cancers to oestrogen deprivation. *Nat Commun*  
392 7:13294, 2016
- 393 5. Giltane JM, Hutchinson KE, Stricker TP, et al: Genomic profiling of ER+ breast  
394 cancers after short-term estrogen suppression reveals alterations associated with endocrine  
395 resistance. *Sci Transl Med* 9, 2017

396 6. McGranahan N, Burrell RA, Endesfelder D, et al: Cancer chromosomal  
397 instability: therapeutic and diagnostic challenges. *EMBO Rep* 13:528-38, 2012

398 7. Swanton C, Nicke B, Schuett M, et al: Chromosomal instability determines  
399 taxane response. *Proc Natl Acad Sci U S A* 106:8671-6, 2009

400 8. Dowsett M, Smith IE, Ebbs SR, et al: Prognostic value of Ki67 expression after  
401 short-term presurgical endocrine therapy for primary breast cancer. *J Natl Cancer Inst*  
402 99:167-70, 2007

403 9. Ellis MJ, Suman VJ, Hoog J, et al: Ki67 Proliferation Index as a Tool for  
404 Chemotherapy Decisions During and After Neoadjuvant Aromatase Inhibitor Treatment of  
405 Breast Cancer: Results From the American College of Surgeons Oncology Group Z1031 Trial  
406 (Alliance). *J Clin Oncol* 35:1061-1069, 2017

407 10. Dowsett M, Smith IE, Ebbs SR, et al: Short-term changes in Ki-67 during  
408 neoadjuvant treatment of primary breast cancer with anastrozole or tamoxifen alone or  
409 combined correlate with recurrence-free survival. *Clin Cancer Res* 11:951s-8s, 2005

410 11. Dowsett M, Smith I, Robertson J, et al: Endocrine therapy, new biologicals, and  
411 new study designs for presurgical studies in breast cancer. *J Natl Cancer Inst Monogr*  
412 2011:120-3, 2011

413 12. Van Loo P, Nordgard SH, Lingjaerde OC, et al: Allele-specific copy number  
414 analysis of tumors. *Proc Natl Acad Sci U S A* 107:16910-5, 2010

415 13. Yau C, Mouradov D, Jorissen RN, et al: A statistical approach for detecting  
416 genomic aberrations in heterogeneous tumor samples from single nucleotide polymorphism  
417 genotyping data. *Genome Biol* 11:R92, 2010

418 14. Quinlan AR, Hall IM: BEDTools: a flexible suite of utilities for comparing  
419 genomic features. *Bioinformatics* 26:841-2, 2010

420 15. Lopez-Knowles E, Gao Q, Cheang MC, et al: Heterogeneity in global gene  
421 expression profiles between biopsy specimens taken peri-surgically from primary ER-positive  
422 breast carcinomas. *Breast Cancer Res* 18:39, 2016

423 16. Benjamini Y, Hochberg Y: Controlling the False Discovery Rate: A Practical and  
424 Powerful Approach to Multiple Testing. *Journal of the Royal Statistical Society. Series B*  
425 (Methodological) 57:289-300, 1995

426 17. Cancer Genome Atlas N: Comprehensive molecular portraits of human breast  
427 tumours. *Nature* 490:61-70, 2012

428 18. Pereira B, Chin SF, Rueda OM, et al: The somatic mutation profiles of 2,433  
429 breast cancers refines their genomic and transcriptomic landscapes. *Nat Commun* 7:11479,  
430 2016

431 19. Haricharan S, Punturi N, Singh P, et al: Loss of MutL Disrupts CHK2-Dependent  
432 Cell-Cycle Control through CDK4/6 to Promote Intrinsic Endocrine Therapy Resistance in  
433 Primary Breast Cancer. *Cancer Discov* 7:1168-1183, 2017

434 20. Quenel-Tueux N, Debled M, Rudewicz J, et al: Clinical and genomic analysis of a  
435 randomised phase II study evaluating anastrozole and fulvestrant in postmenopausal patients  
436 treated for large operable or locally advanced hormone-receptor-positive breast cancer. *Br J*  
437 *Cancer* 113:585-94, 2015

438 21. Bilal E, Dutkowski J, Guinney J, et al: Improving breast cancer survival analysis  
439 through competition-based multidimensional modeling. *PLoS Comput Biol* 9:e1003047, 2013

440 22. Margolin AA, Bilal E, Huang E, et al: Systematic analysis of challenge-driven  
441 improvements in molecular prognostic models for breast cancer. *Sci Transl Med* 5:181re1,  
442 2013

443 23. Silwal-Pandit L, Vollan HK, Chin SF, et al: TP53 mutation spectrum in breast  
444 cancer is subtype specific and has distinct prognostic relevance. *Clin Cancer Res* 20:3569-80,  
445 2014

- 446 24. Curtis C, Shah SP, Chin SF, et al: The genomic and transcriptomic architecture of  
447 2,000 breast tumours reveals novel subgroups. *Nature* 486:346-52, 2012
- 448 25. Haricharan S, Bainbridge MN, Scheet P, et al: Somatic mutation load of estrogen  
449 receptor-positive breast tumors predicts overall survival: an analysis of genome sequence  
450 data. *Breast Cancer Res Treat* 146:211-20, 2014
- 451 26. Dowsett M, Nielsen TO, A'Hern R, et al: Assessment of Ki67 in breast cancer:  
452 recommendations from the International Ki67 in Breast Cancer working group. *J Natl Cancer*  
453 *Inst* 103:1656-64, 2011
- 454

455 **Figure Legends:**

456 **Figure 1.**

457 **A.** Arrow plot showing the change in Ki67 between baseline and surgery for GdRs (green),  
458 PrRs (red) and untreated Controls (blue). **B.** Boxplot showing percent of the genome with  
459 SCNAs, gains relative tumor ploidy, losses relative to tumor ploidy, LOH and HD for 127  
460 tumor samples (PrRs in red, GdRs in green and controls in blue). Barplot **(C)** and boxplot  
461 **(D)** showing the average percentage of genome discordant between pairs of core-cuts  
462 (baseline and surgery) for all SCNAs (GdRs - green, PrRs - red and untreated Controls -  
463 blue).

464

465 **Figure 2.**

466 Boxplot showing the difference in GI (the percentage of genome with SCNAs) between  
467 GdRs (green) and PrRs (red) tumors **(A)**. Comparisons of Ki67 baseline IHC scores with  
468 GI (the percent of the genome with SCNAs). **B.** for GdRs (green circles), PrRs (red  
469 squares) and untreated Controls (light blue squares). Comparisons of Ki67 surgery IHC  
470 scores after AI treatment with GI (the percent of the genome with with SCNAs). **C.** PrRs  
471 (red squares) and GdRs (green circles). Grey lines represent regression line.

472

473

474 **Figure 3.**

475 Percentage of samples with gains relative to tumor ploidy for PrRs (dark red) and GdRs  
476 (pink) (**A**), with losses (light blue – GdR, dark blue – PrR) (**B**) and with LOH (light green  
477 GdR, dark green – PrR) (**C**) at 47807 segments generated from POETIC SCNA analysis.  
478 Percentage of samples with LOH (light green GdRs, dark green – PrRs) for chromosome  
479 17 (**D**) including table for LOH events at *TP53* (**E**) and difference in the % of samples with  
480 LOH between PrRs and GdRs (**F**). Boxplots showing the percent of 17p with LOH for  
481 GdRs (green) and PrRs (red) (**G**) and barplots showing the percent of LOH at 17p for each  
482 tumor (PrRs –red, GdRs – green) (**H**).

483

#### 484 **Figure 4.**

485 **A.** Barplot showing percentage of GdR (green) and PrR (red) samples with *TP53*<sup>WT</sup> and no  
486 LOH at the *TP53* locus, *TP53*<sup>WT</sup> and LOH at the *TP53* locus, *TP53*<sup>MUT</sup> and no LOH at the  
487 *TP53* locus and *TP53*<sup>MUT</sup> and LOH at the *TP53* locus. Note: One GrR does not have  
488 exome sequencing data. Boxplot showing the % change in Ki67 (**B**), Ki67 baseline scores  
489 (**C**), Ki67 surgery score (**D**) and GI (the percentage of the genome with SCNAs) (**E**) for  
490 PrRs with *TP53*<sup>WT</sup> and no LOH at the *TP53* locus, *TP53*<sup>WT</sup> and LOH at the *TP53* locus,  
491 and *TP53*<sup>MUT</sup> and LOH at the *TP53* locus. There are no PrR samples with *TP53*<sup>MUT</sup> and no  
492 LOH at the *TP53* locus.

493

#### 494 **Supplemental Tables/Figures**

495 **Supplemental Table 1.** Clinical, Ki67 and genomic data for 127 tumors in study.

496 **Supplemental Table 2.** ASCAT estimates and segments for 127 Tumors in study.

497

498 **Supplemental Figure 1.** Consort Diagram.

499 **Supplemental Figure 2.** Percent of representative tumors from each of the 73 patients  
500 with gains, losses or LOH and overlaps between segments. Percentage of discordance for  
501 technical and biological replicates.

502 **Supplemental Figure 3.** ASCAT estimates of SCNA gains, losses and LOH for 127  
503 tumors.

504 **Supplemental Figure 4.** Percentage of gains, losses and LOH for 33 AI treated pairs.

505 **Supplemental Figure 5.** Percentage of genome with SCNAs and discordance.

506 **Supplemental Figure 6.** Independent tumors from same patient.

507 **Supplemental Figure 7.** Chromosomal arm analysis of gains, losses and LOH.

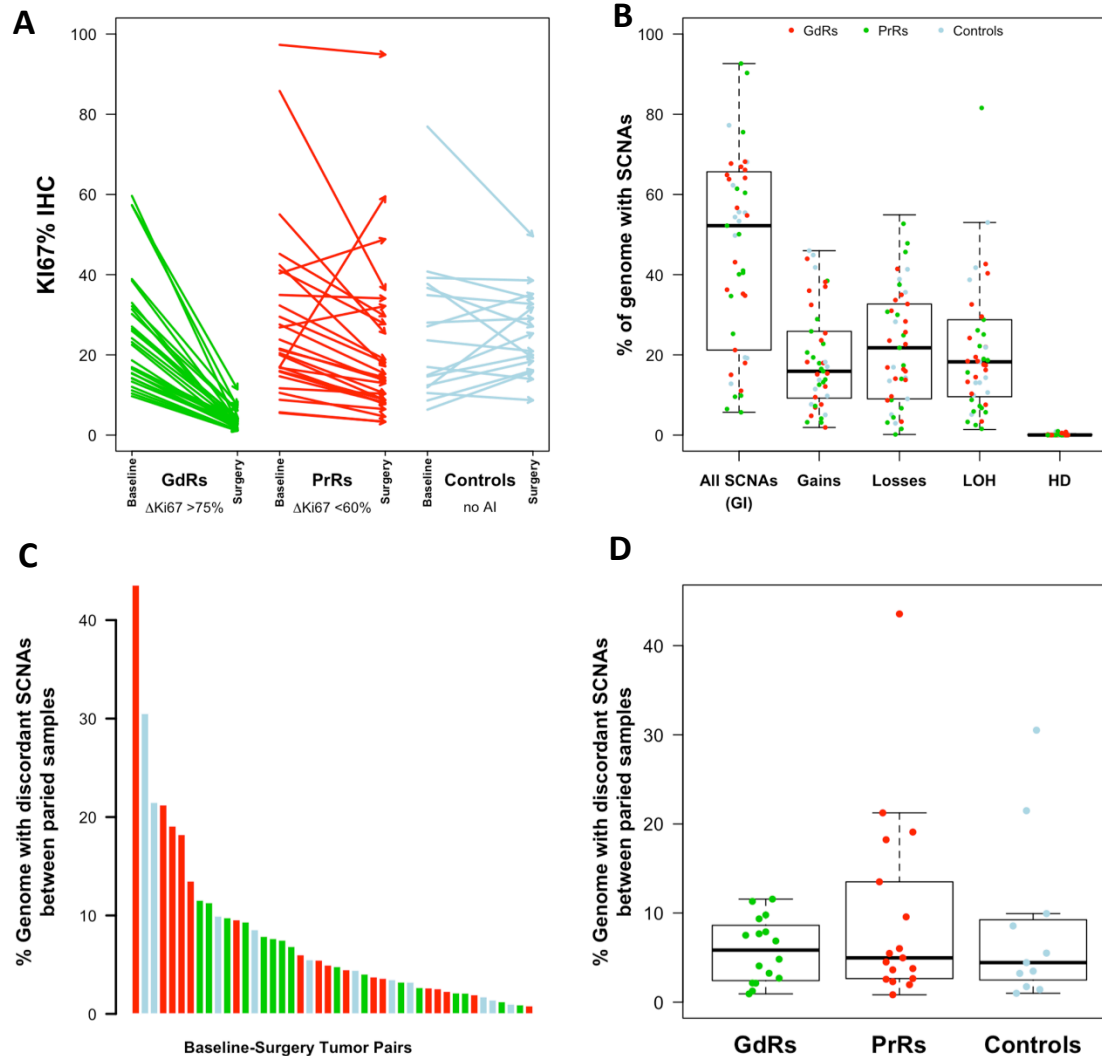
508 **Supplemental Figure 8.** Differences in percentage of samples with gains, losses and  
509 LOH with and without HER2 positive samples.

510 **Supplemental Figure 9.** Differences in percentage of samples with SCNAs when  
511 including or excluding HER2 positive tumors.

512 **Supplemental Figure 10.** Differences in percentage of samples with LOH at 17p when  
513 including or excluding HER2 positive tumors.

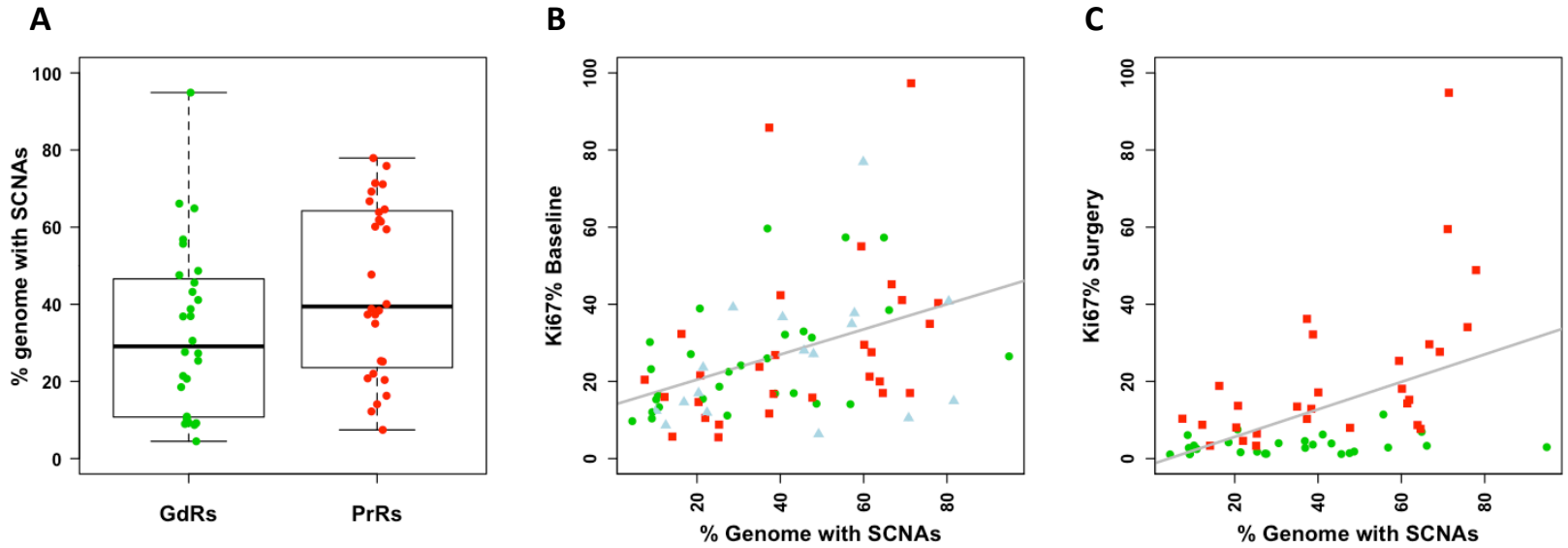
514 **Supplemental Figure 11.** Breast cancer-specific survival (BCSS) survival plots for  
515 METABRIC LumA stratified by *TP53* mutation.

Figure 1



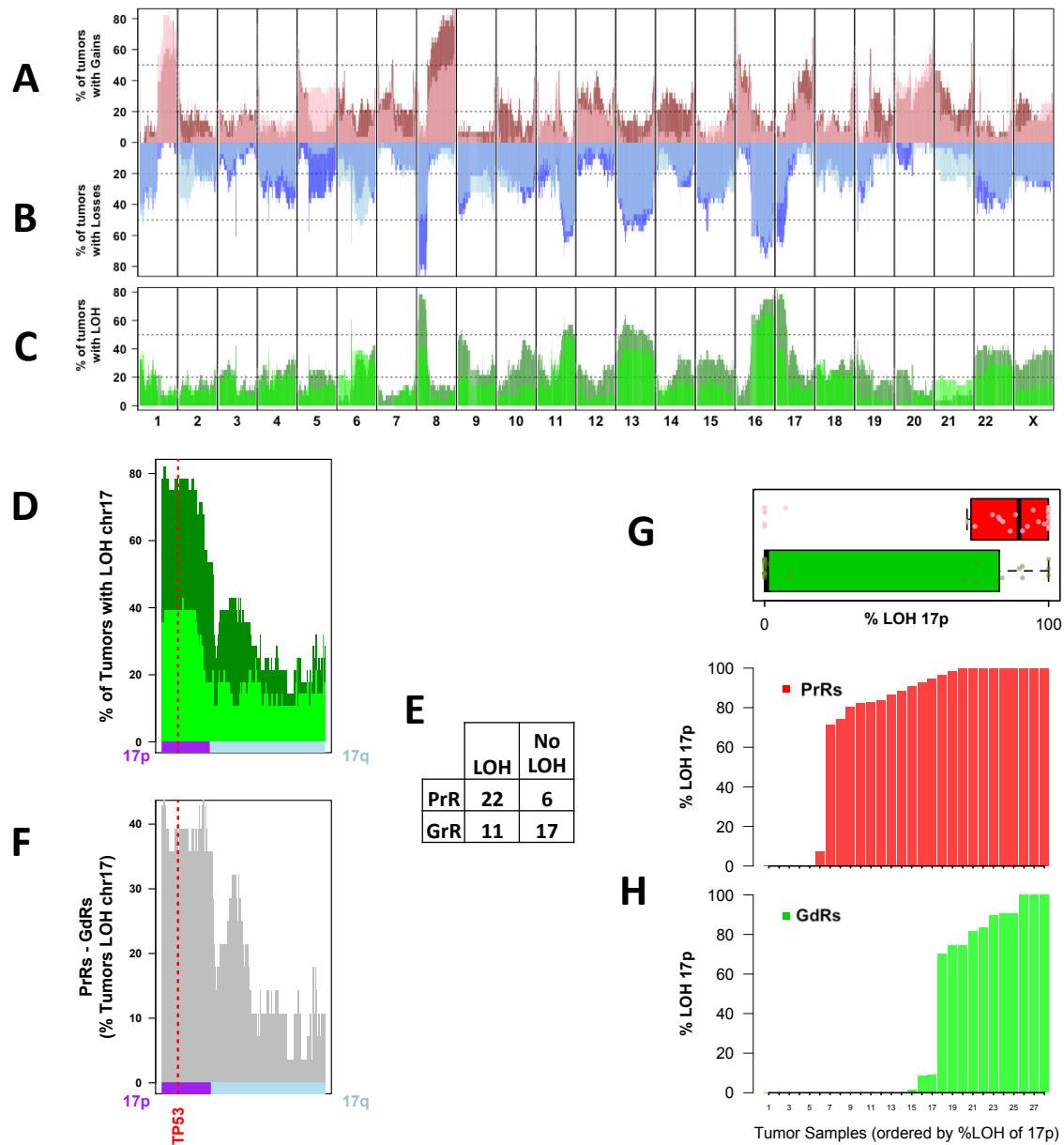
**Figure 1. A.** Arrow plot showing the change in Ki67 between baseline and surgery for GdRs (green), PrRs (red) and untreated Controls (blue). **B.** Boxplot showing percent of the genome with SCNAs, gains relative tumor ploidy, losses relative to tumor ploidy, LOH and HD for 127 tumor samples (PrRs in red, GdRs in green and controls in blue). Barplot (**C**) and boxplot (**D**) showing the average percentage of genome discordant between pairs of core-cuts (baseline and surgery) for all SCNAs (GdRs - green, PrRs - red and untreated Controls - blue).

Figure 2



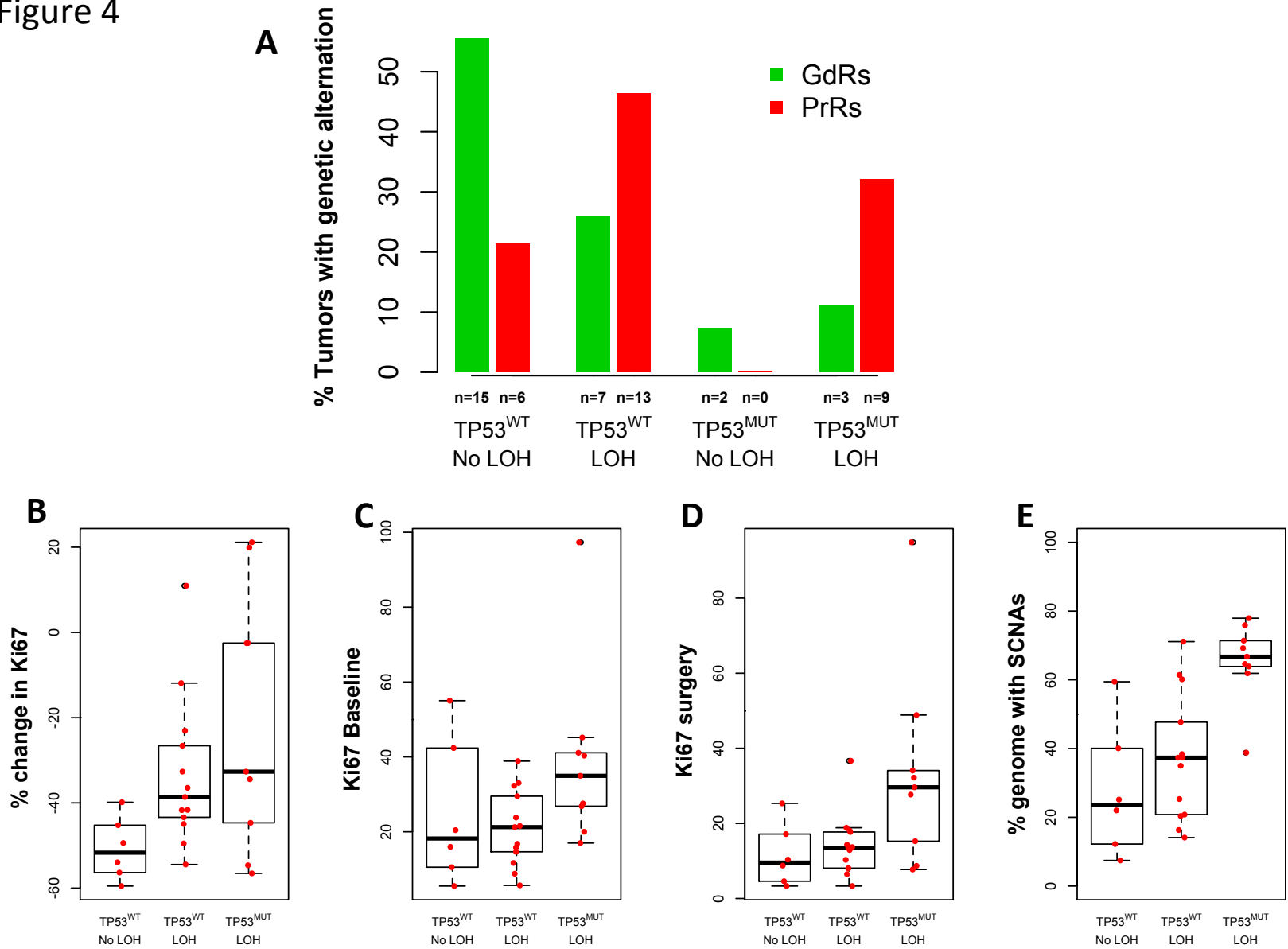
**Figure 2.** Boxplot showing the difference in GI (the percentage of genome with SCNAs) between GdRs (green) and PrRs (red) tumors (A). Comparisons of Ki67 baseline IHC scores with GI (the percent of the genome with SCNAs) (B) for GdRs (green circles), PrRs (red squares) and untreated Controls (light blue squares). Comparisons of Ki67 surgery IHC scores after AI treatment with GI (the percent of the genome with with SCNAs) (C) PrRs (red squares) and GdRs (green circles). Grey lines represent regression line.

Figure 3



**Figure 3.** Percentage of samples with gains relative to tumor ploidy for PrRs (dark red) and GdRs (pink) (A), with losses (light blue – GdR, dark blue – PrR) (B) and with LOH (light green GdR, dark green – PrR) (C) at 47807 segments generated from POETIC SCNA analysis. Percentage of samples with LOH (light green GdRs, dark green – PrRs) for chromosome 17 (D) including table for LOH events at *TP53* (E) and difference in the % of samples with LOH between PrRs and GdRs (F). Boxplots showing the percent of 17p with LOH for GdRs (green) and PrRs (red) (G) and barplots showing the percent of LOH at 17p for each tumor (PrRs –red, GdRs –green) (H).

Figure 4



**Figure 4. A.** Barplot showing percentage of GdR (green) and PrR (red) samples with  $TP53^{WT}$  and no LOH at the  $TP53$  locus,  $TP53^{WT}$  and LOH at the  $TP53$  locus,  $TP53^{MUT}$  and no LOH at the  $TP53$  locus and  $TP53^{MUT}$  and LOH at the  $TP53$  locus. Note: One GrR does not have exome sequencing data. Boxplot showing the % change in Ki67 (**B**), Ki67 baseline scores (**C**), Ki67 surgery score (**D**) and GI (the percentage of the genome with SCNAs) (**E**) for PrRs with  $TP53^{WT}$  and no LOH at the  $TP53$  locus,  $TP53^{WT}$  and LOH at the  $TP53$  locus, and  $TP53^{MUT}$  and LOH at the  $TP53$  locus. There are no PrR samples with  $TP53^{MUT}$  and no LOH at the  $TP53$  locus.

**Supplemental Figure 1**

**73 Patients with DNA extractions  
192 samples (73 blood, 67 baseline and 62 surgery)**

**202 samples hybridised  
Illumina OmniExpressExome-8 v3**

**Allele-Specific Copy number Analysis of Tumours  
(ASCAT) SCNAs Analysis**

**5 blood samples failed QC and replaced  
with germline genotype predictions**

**2 tumour samples failed QC  
(2 baseline samples, 1 Good and 1 Poor)**

**Good Responders (GdRs): 28  
Ki67% change after AI 2wks > 75%**

**Poor Responders (PrRs): 28  
Ki67% change after AI 2wks < 60%**

**Controls: 17  
No AI treatment**

**Baseline only: 6  
(1 with technical replicate)**

**Surgery only: 6**

**Pairs: 16  
(2 with baseline, 1 with surgery  
technical replicates)**

**Baseline only: 8**

**Surgery only: 3**

**Pairs: 17  
(3 with baseline, 1 with surgery  
technical replicate)**

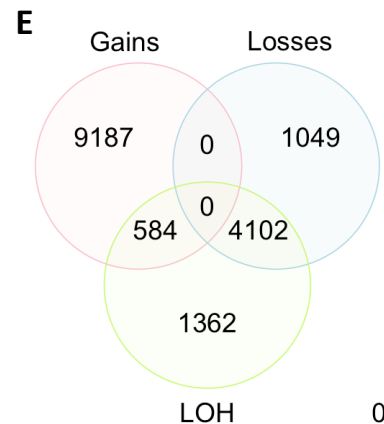
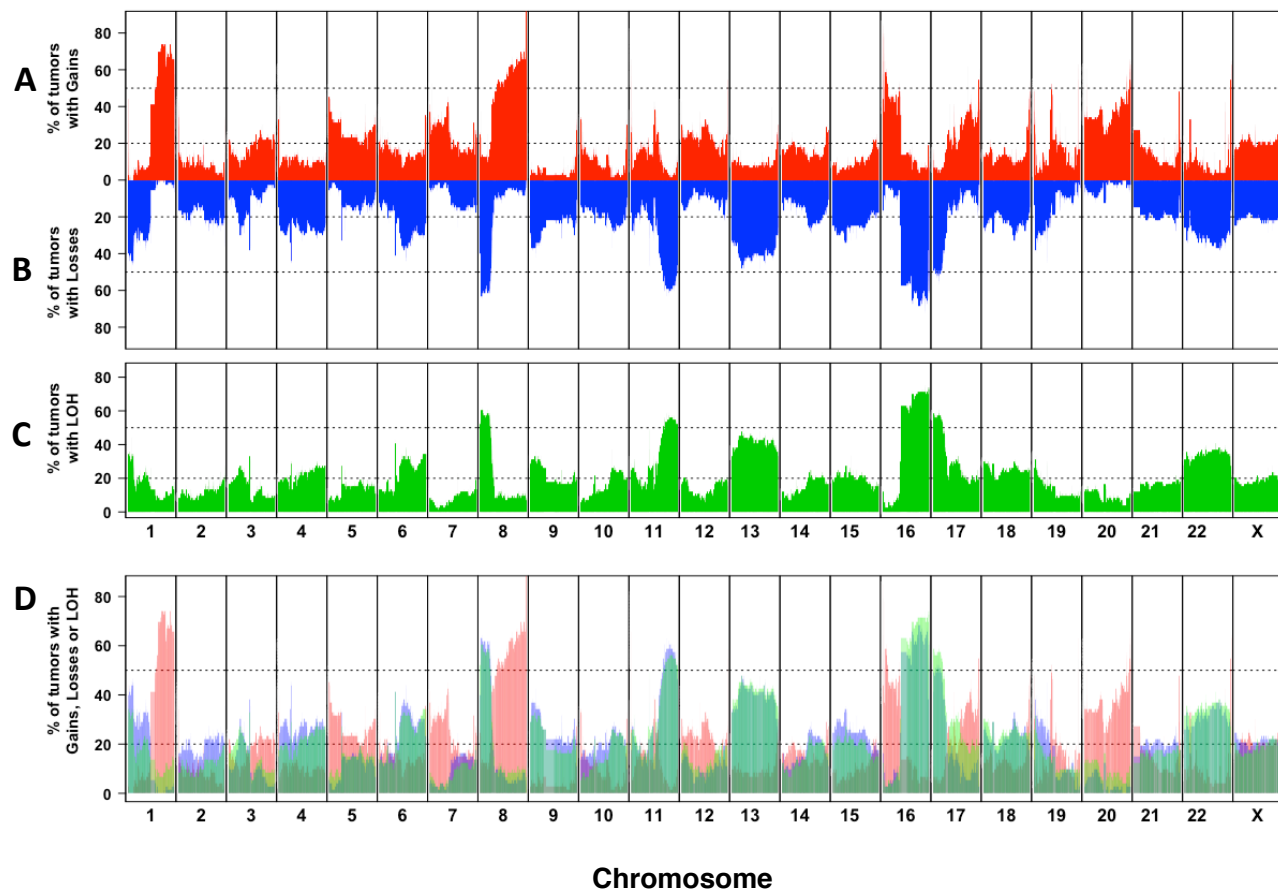
**Baseline only: 2**

**Surgery only: 4**

**Pairs: 11  
(2 with surgery technical replicates)**

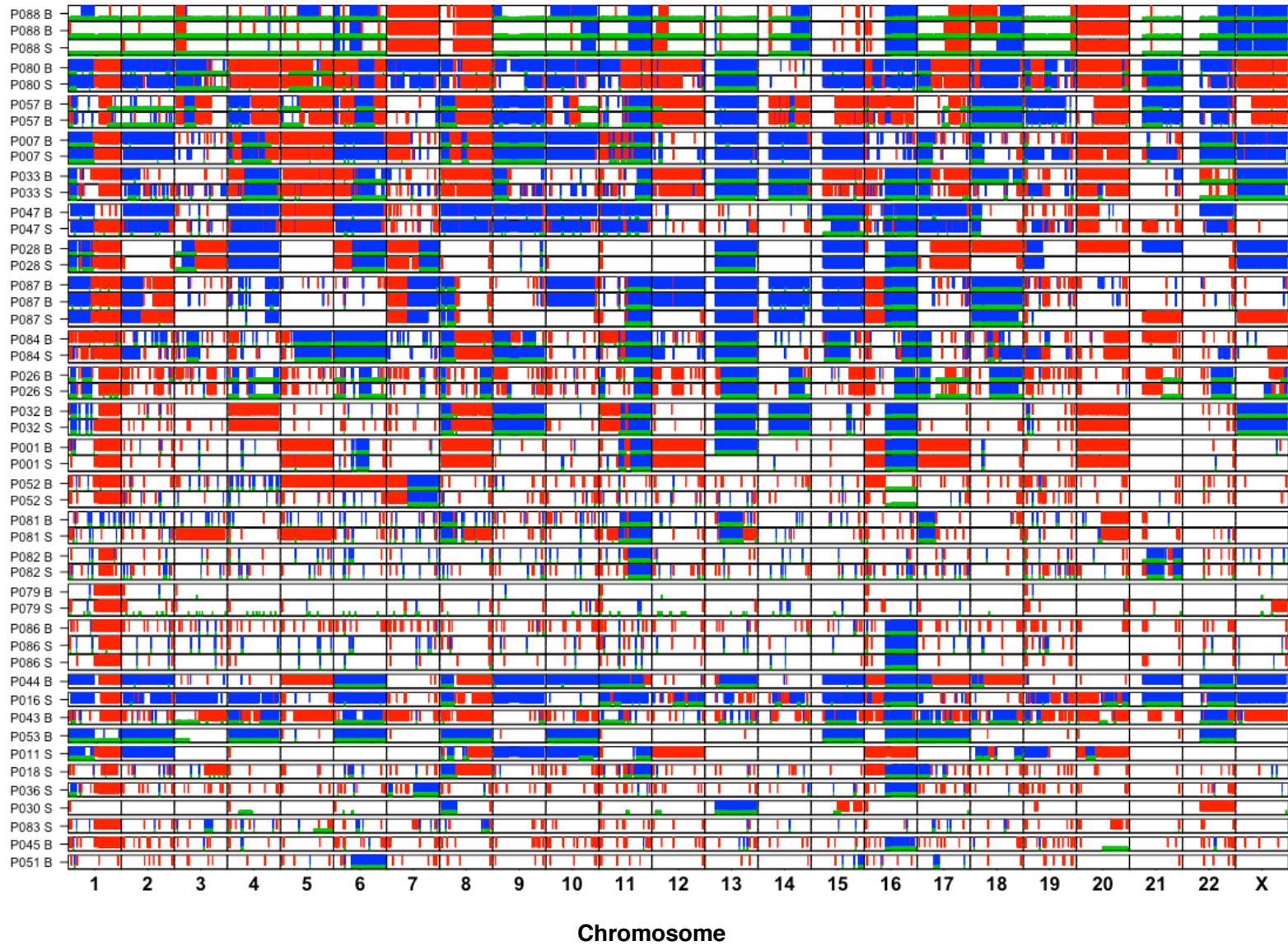
Supplemental Figure 1. Consort Diagram.

# Supplemental Figure 2

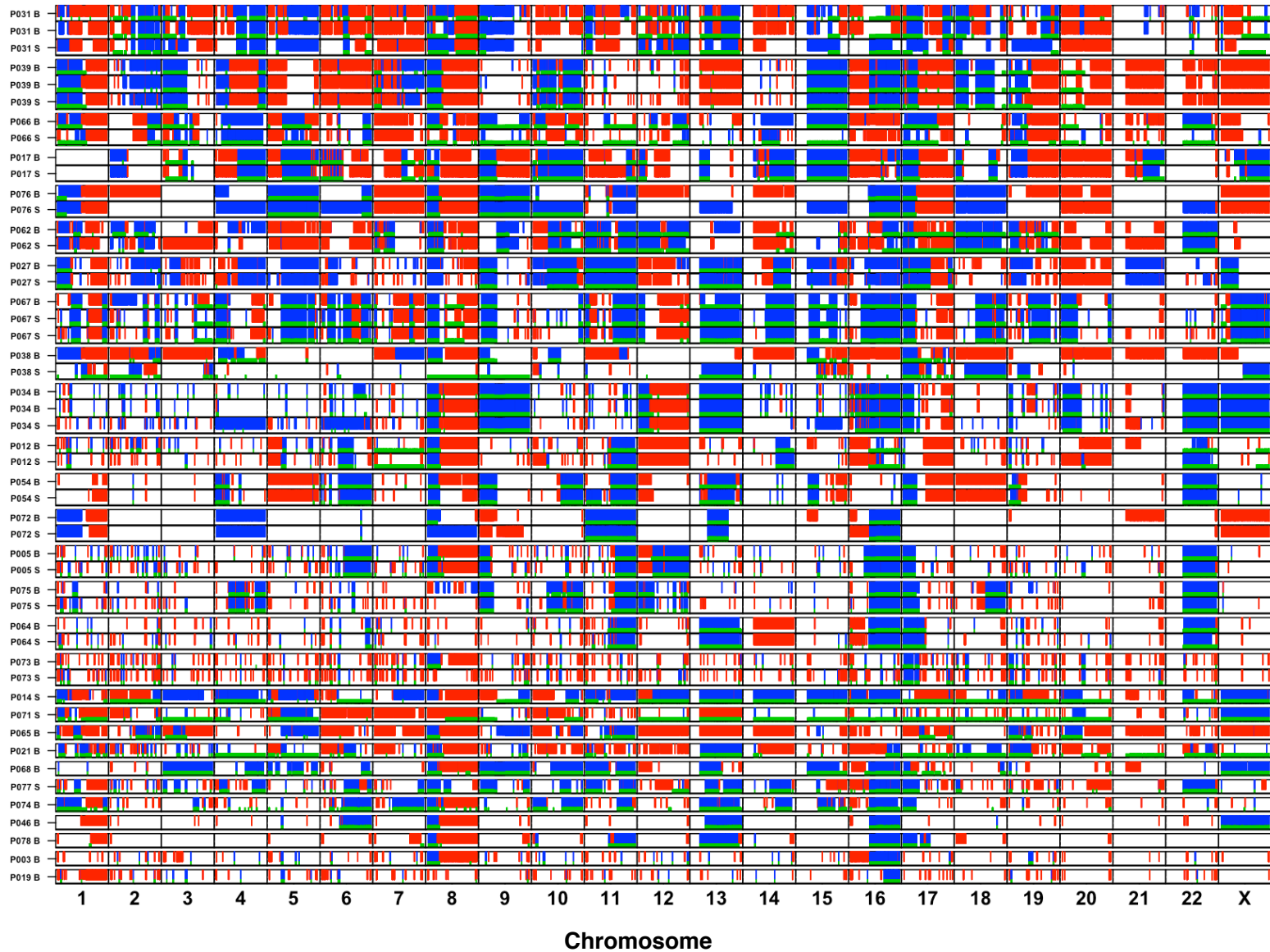


Supplemental Figure 2. Percent of representative tumors from each of the 73 patients with gains (A), losses (B) or LOH (C) for each of 47807 bedtool segments separated by chromosome. Segments generated by integrating all ASCAT output segments for all tumor samples with bedtools multiintersect tool. For patients with multiple tumor samples, representative tumor was randomly chosen. Plot (D) showing percent of tumors with gains (red), losses (blue) and LOH (green) for each segment from Supplemental Figures 1B-D. Venn diagram (E) showing the overlap between gains, losses and LOH of ASCAT output segments from representative tumors of all 73 patients.

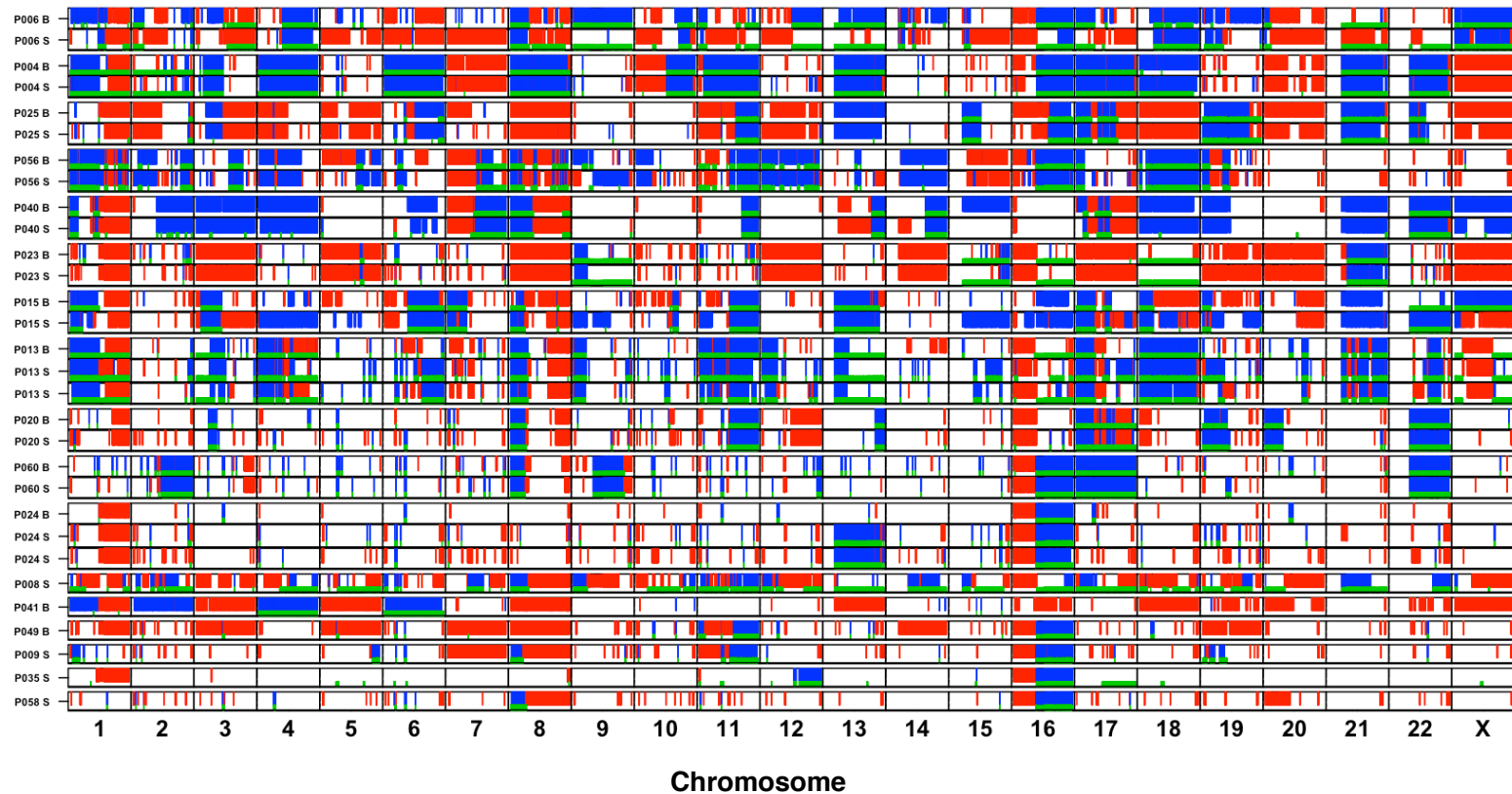
# Supplemental Figure 3A



# Supplemental Figure 3B

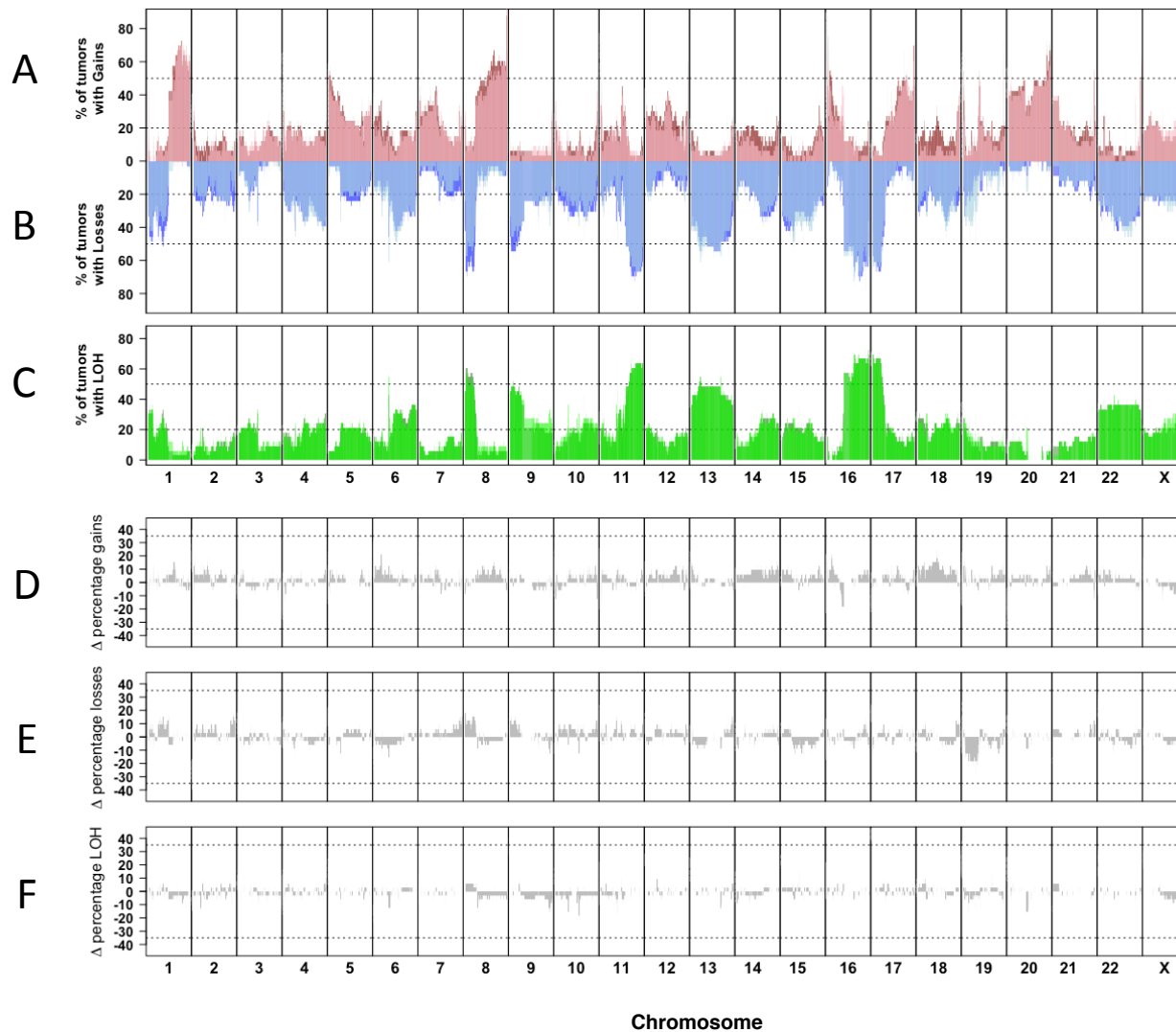


# Supplemental Figure 3C



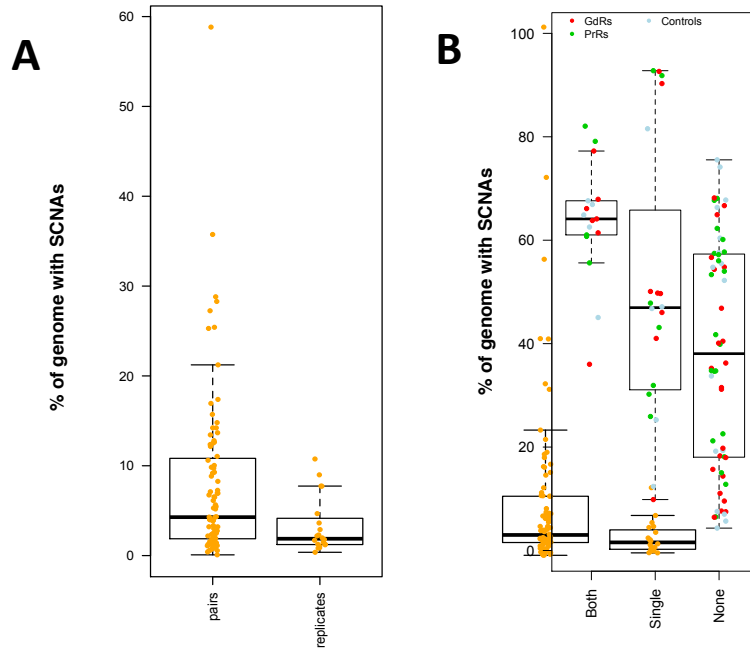
Supplemental Figure 3. ASCAT estimates of SCNA gains (red) and losses (blue) relative to tumour ploidy for GdRs (A), PrRs (B) and Control samples (C) for baseline and surgery samples. Green bars represent regions with LOH. Label to right of figure shows sample ID and timepoint of biopsy (B – Baseline and S – Surgery). Samples with baseline and surgery pairs or replicate samples are grouped together at top of figures.

# Supplemental Figure 4



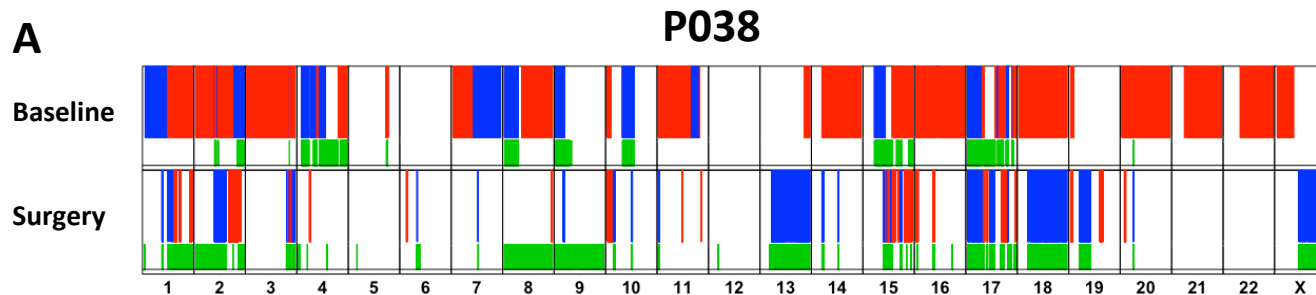
Supplemental Figure 4. Percentage of 33 AI treated pairs with gains relative to tumour ploidy (A) in baseline (dark red) and surgery (pink) samples, with losses relative to tumor ploidy (B) in baseline (dark blue) and surgery (light blue) samples, and with LOH (C) in baseline (dark green) and surgery (light green) samples. Difference in the percentage of SCNA gains (D), losses (E) and LOH (F) between surgery and baseline samples (% surgery SCNA - % baseline SCNA).

## Supplemental Figure 5

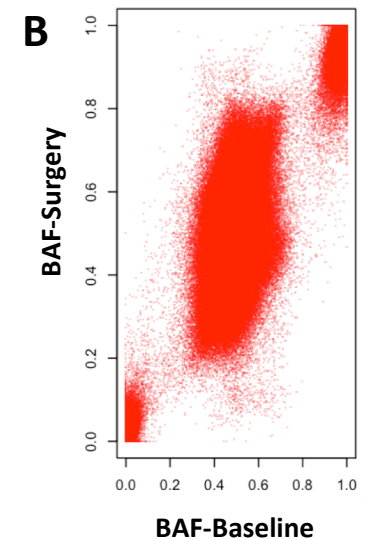


Supplemental Figure 5. A. Boxplot showing percent of genome with SCNAs that are exclusive to one sample from a pair of baseline and surgery samples or from technical replicate samples taken from the same timepoint. B. Boxplot showing GI (percent of genome with SCNAs) for samples in which both samples in the baseline-surgery pair were observed to have exclusive SCNAs that covered at least 10% of the genome (Both), samples in which only one sample in the pair was observed to have exclusive SCNAs that covered at least 10% of the genome (Single) or none of the samples in the pairs had exclusive SCNAs covering more than 10% of the genome (None).

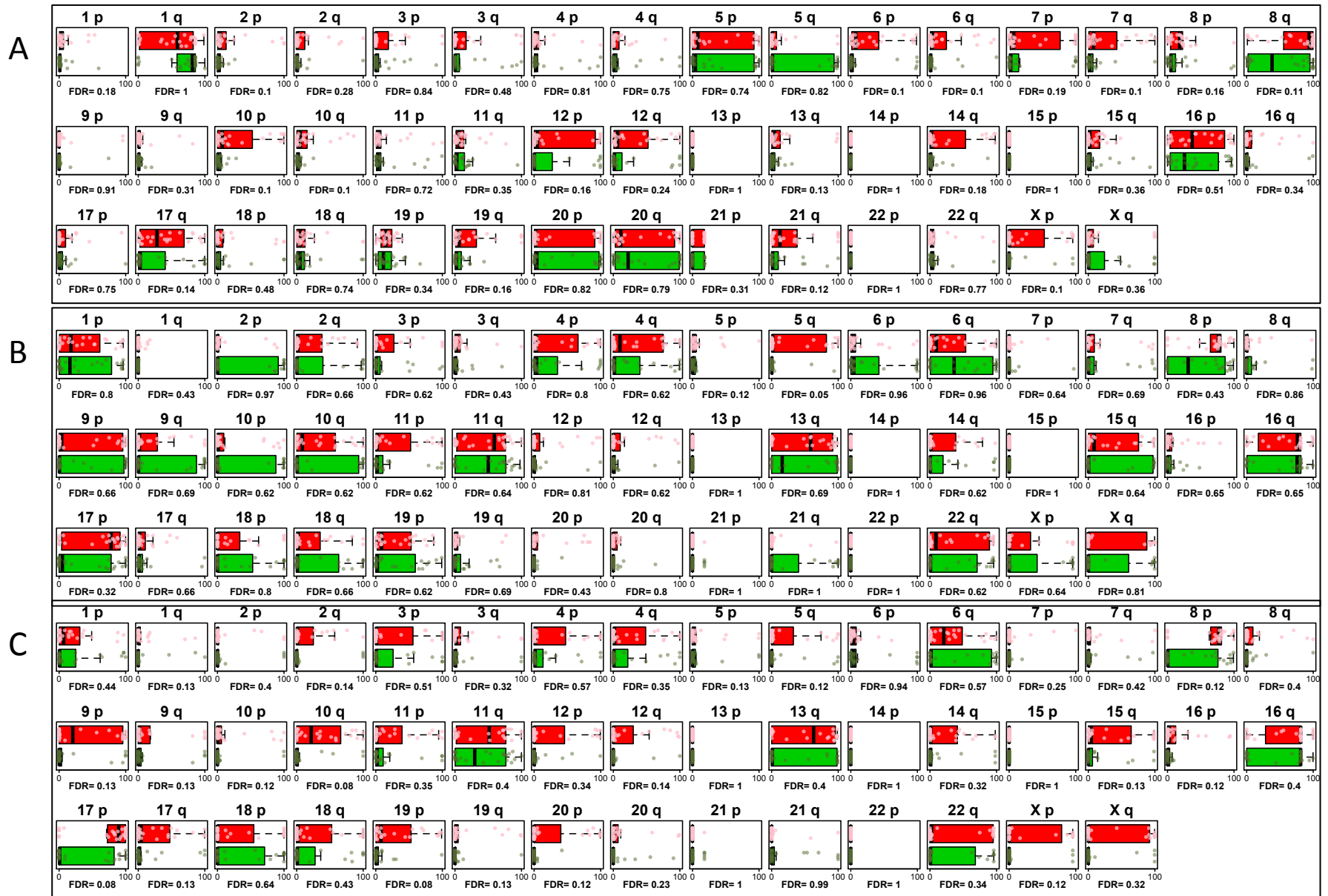
## Supplemental Figure 6



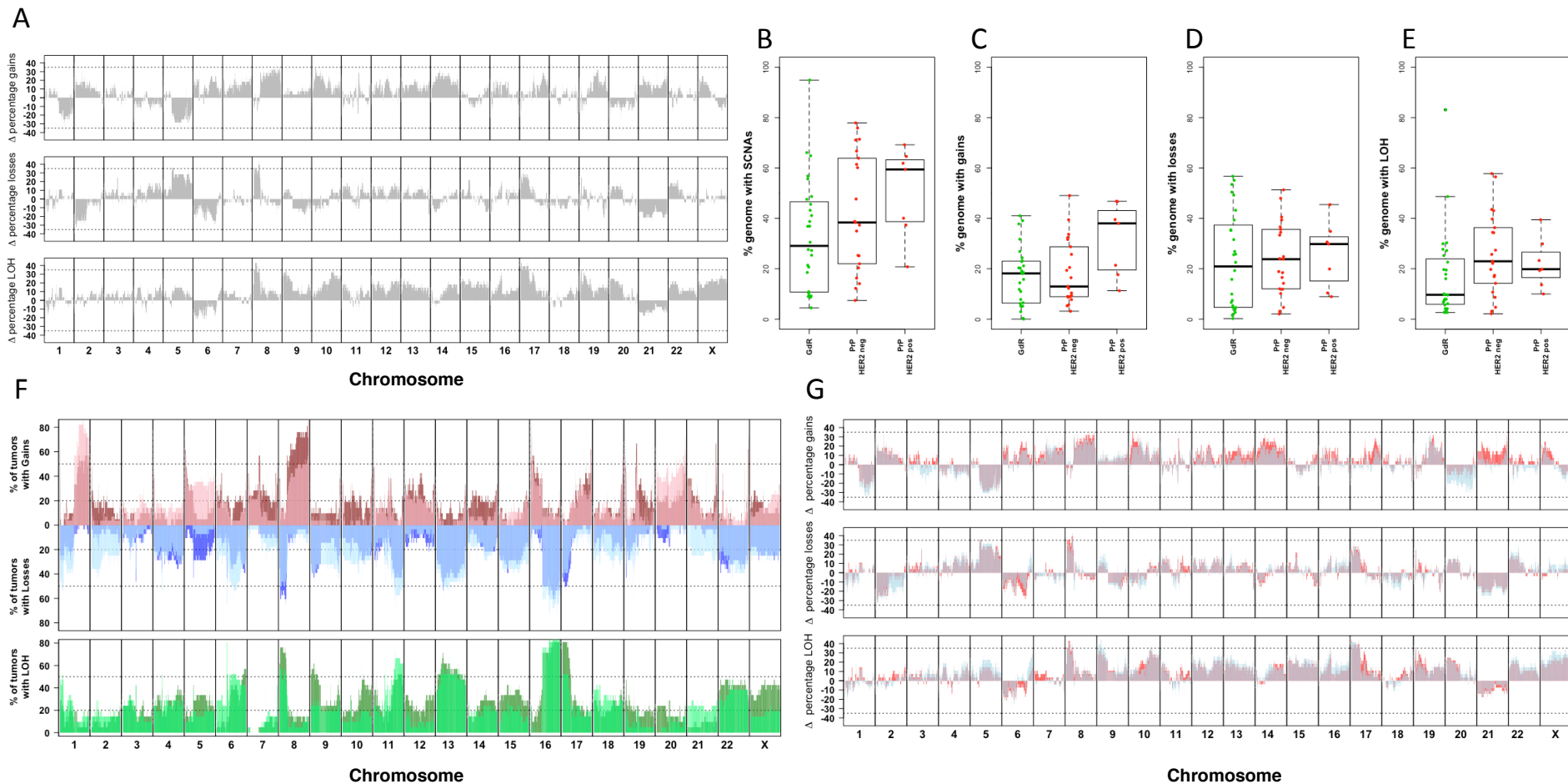
Supplemental Figure 6. A. ASCAT estimates of SCNA gains (red) and losses (blue) relative to tumour ploidy and regions with LOH (green) in paired set of core-cuts in which the SCNAs exclusive to the baseline and surgery sample are greater than the SCNAs shared between the pair of samples. B. Comparison of B or Minor allele frequencies (BAF) for baseline and surgery biopsy samples showing the tumor biopsies are from the same individual as there is a very high concordance for alleles to be either homozygous or heterozygous in both samples.



# Supplemental Figure 7

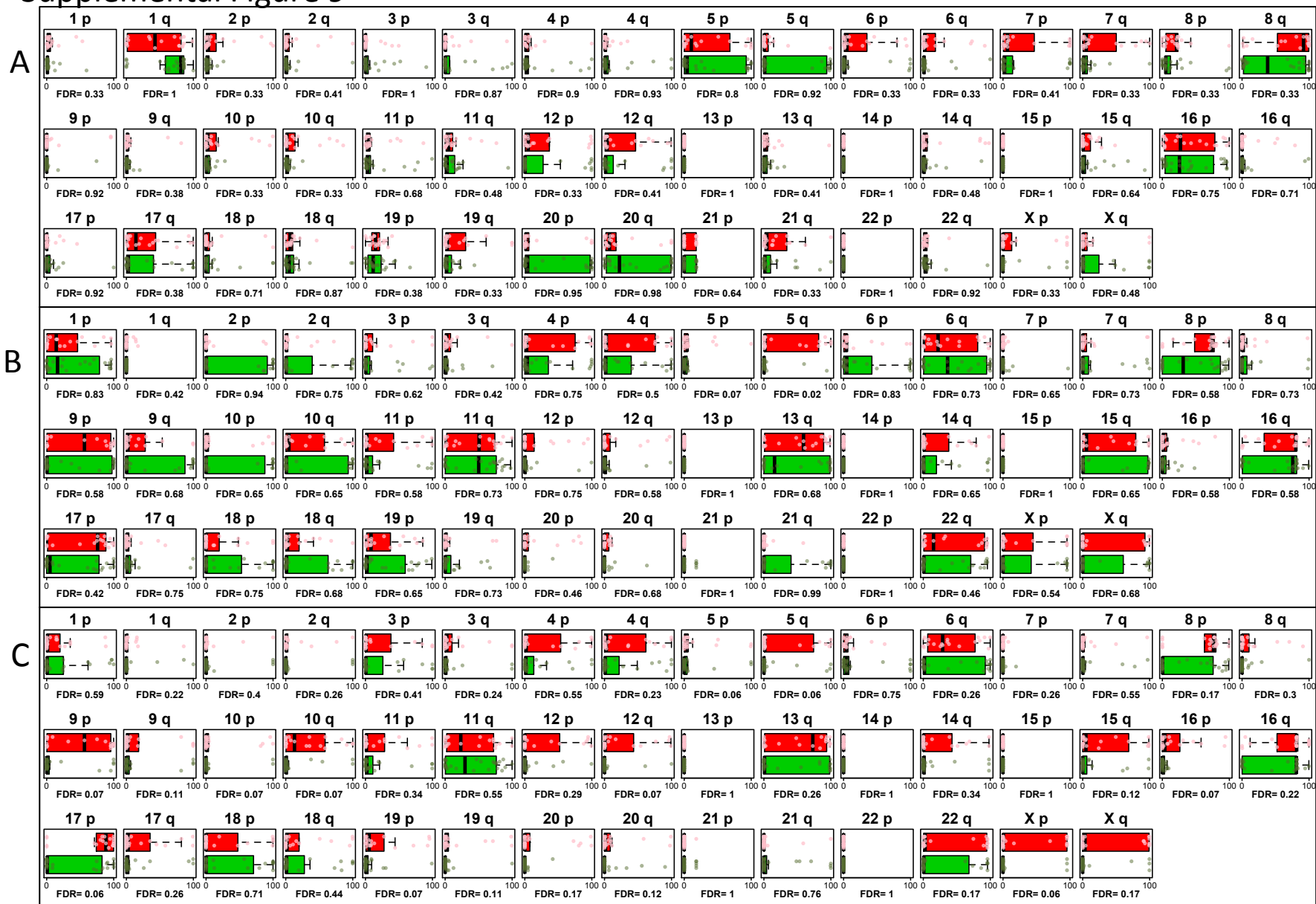


# Supplemental Figure 8



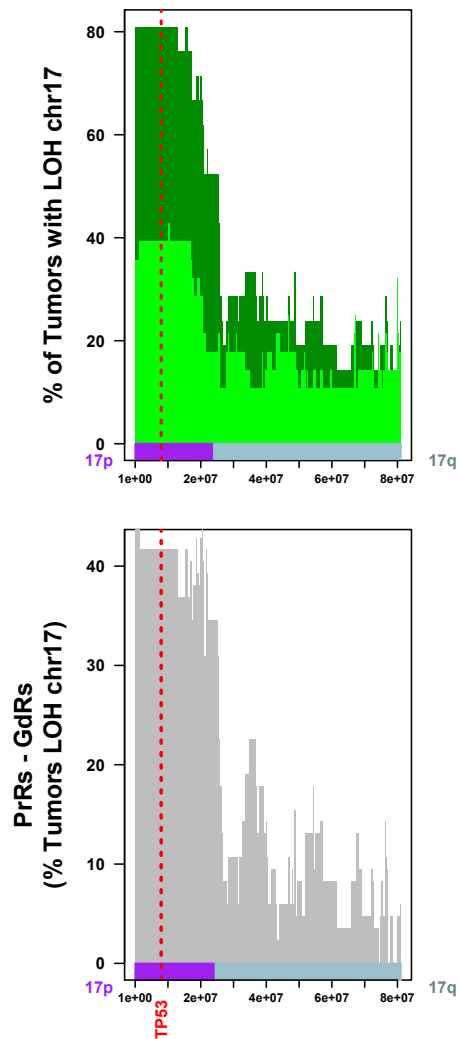
Supplemental Figure 8. Difference in the percentage of SCNA gains, losses and LOH (A) between PrR and GdR samples (% PrR SCNA - % GdR SCNA). Boxplot showing percent of genome with SCNAs (B), gains (C), losses (D) and LOH (E) for GdRs, PrRs that are HER2 negative and PrRs that are HER2 positive. Percentage of samples with gains relative to tumour ploidy for PrRs (dark red) and GdRs (pink), with losses (light blue – GdR, dark blue – PrR) and with LOH (light green GdR, dark green – PrR) at 47807 bedtool segments generated from POETIC SCNA analysis with HER2 positive samples removed. Difference in the percentage of SCNA gains, losses and LOH (G) between PrR and GdR samples (% PrR SCNA - % GdR SCNA) including (red) or excluding (light blue) HER2 positive samples.

# Supplemental Figure 9



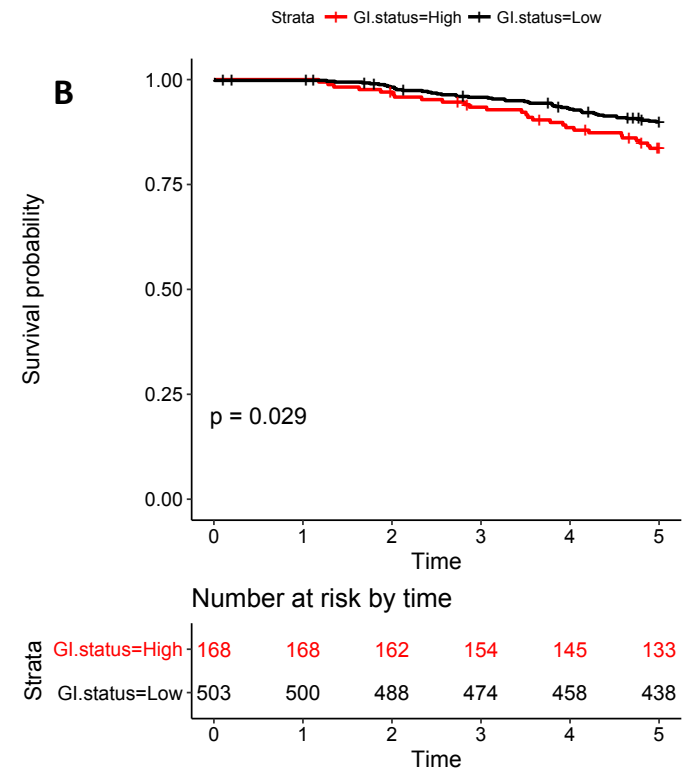
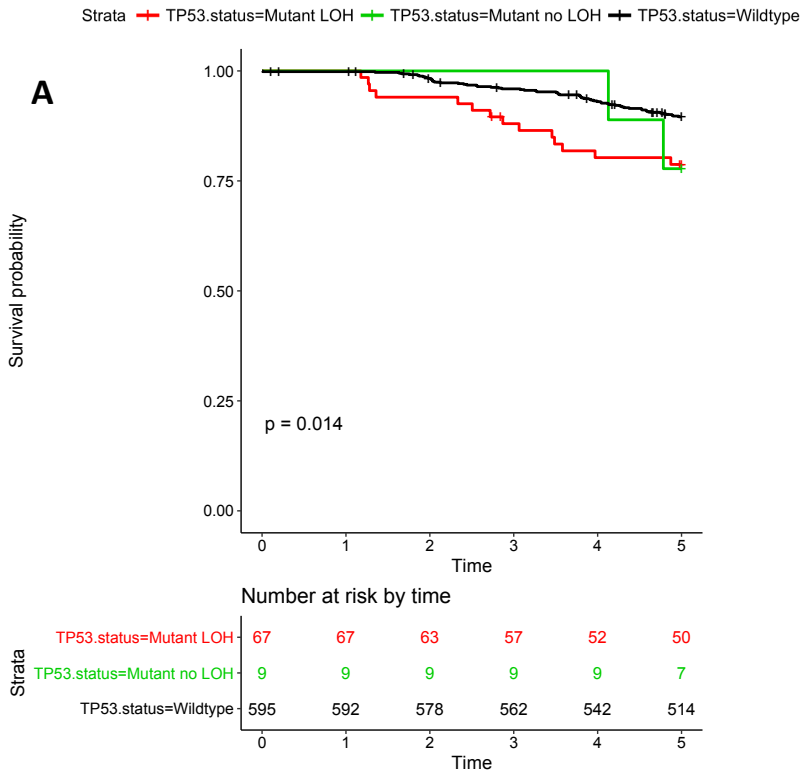
Supplemental Figure 9. Boxplots showing the percent of each chromosomal arm with gains (A), losses (B) and LOH (C) for GdRs (green) and PrRs (red) for HER2-negative tumors. Significance of difference between PrRs and GdRs based on Mann-Whitney tests (one sided) after multiple correction (FDR BH) is also shown.

## Supplemental Figure 10



Supplemental Figure 10. Percentage of samples with LOH (light green GdR, dark green – PrR) for chromosome 17 (A) and difference in the % of samples with LOH between PrRs and GdRs (B). HER2 positives samples were removed from the PrR samples.

# Supplemental Figure 11



Supplemental Figure 11. Breast cancer-specific survival (BCSS) survival plots for METABRIC LumA stratified by *TP53* mutation (**A**) and GI (**B**). Samples in the top 25% of GI for LumA tumors (>35% of genome with SCNAs) were defined as having high GI (red). Kaplan-Meier survival curve analysis was performed in R (version 3.2.3) with survfit function from the survival package and survival plots generated with ggsurvplot function from the survminer package.